



## Hybrid Templating Approach for the Synthesis of Hierarchical Oxides: Titania Heterojunctions for Photodegradation of Organic Dyes

Maryam Fatolah<sup>1</sup>, Gholam Reza Khayati\*<sup>1</sup>, Parham Fatolah<sup>2</sup>

<sup>1</sup>Department of Materials Science and Engineering, Shahid Bahonar University of Kerman, Kerman, Iran;

<sup>2</sup>Department of Materials Engineering, Tarbiat Modares University, Tehran, Iran.

Received: 12 December 2021; Accepted: 8 February 2022

\*Corresponding author email: [Khayatireza@gmail.com](mailto:Khayatireza@gmail.com)

### ABSTRACT

Hierarchical titania with anatase/rutile crystalline phases were obtained by a hybrid hard/soft templating approach. Three sets of conditions were chosen including absolute ethanol, ethanol: water and absolute ethanol with the addition of microcrystalline cellulose as a hard template; in all of the experiments P123 three block co-polymer was utilized as the soft template. Crystallite sizes, porosity and surface acidity were found to change drastically by modifying the initial synthesis conditions. The obtained samples were characterized using powder XRD, FESEM, SEM, TEM, DRS, EDS, N<sub>2</sub>-physisorption, DLS and zeta potential meter. Methyl violet, methyl orange and malachite green were chosen as representative organic pollutants with different chemistries and a series of experiments were performed under a high-pressure mercury lamp equipped with UV filter. It was found that the hierarchical titania sample works best to remove methyl violet from aqueous media while simpler nanostructures obtained with soft templating work better for methyl orange and malachite green. Based on the characterization results, possible enhancement mechanisms were proposed to explain the drastic differences between the performance of different samples for removing different organic dyes.

**Keywords:** Hybrid Templating; Hierarchical; EIS; Photocatalyst

### 1. Introduction

One of the great aims of chemists and materials scientists in the 21<sup>st</sup> century is tackling energy and environmental issues by development of new materials and optimization of the known materials for specific purposes. Effluent discharge into surface water is a major issue that has to be addressed bearing in mind the financial constraints. It has been estimated that about 1-20% of the dyes produced around the world are lost in the coloring process and are released to the environment [1]. Colored pollutants are the most easily detectable of these contaminants, but they pose serious damage to the environment; one particularly critical way is that they absorb and reflect sunlight,

thus photosynthesizing bacteria cannot grow and this in turn impedes the biodegradation of other contaminants [2], add to this the chronic effects on living organisms among other withering phenomena. Advanced oxidation processes have been studied to degrade such pollutants into more benign products [3], among these techniques are the heterogeneous photocatalysts [4].

Titania has been long known as a popular photocatalyst for industrial as well as academic purposes [5]. Long-term chemical stability, suitable band positions, strong oxidizing activity and low cost are added to non-toxicity which is a critical issue for developing environmental remedies that do not pose new dangers on their own accord [6,

7]. As a metastable crystalline phase of titania, anatase has far superior to those of rutile and brookite; this phenomenon has been attributed to low charge recombination rate, high adsorption capacity toward hydroxyl functional group, high surface area do to the inherently small particles and longer life-time of photoinduced charge carriers [7]. One of the most widely used methods for obtaining anatase phase is the sol-gel approach which has been used extensively to obtain high quality ceramics around the world since the mid-1800s till now [8]. A brief summary of selected reports in this area is presented in table 1.

Herein, we report a facile environmentally friendly process classified as an EIS technique in the broader realm of sol-gel synthesis for obtaining hierarchical nanostructures of anatase crystalline phase. Many types of titania photocatalysts are reported to this date but rational pairing between various properties of the photocatalyst and the chemistry of intended pollutants to be degraded are seldom reported. In this study we aim to optimize a simple cost-effective method for obtaining various types of titania nanostructures and pair each of them with a model organic pollutant. Furthermore, we have chosen a high-pressure mercury lamp as the light source which can also be regarded as cost effective due to its widespread use as ambient outside lighting equipment. The benefits of this method include the elimination of harmful chemicals as well as a room temperature

evaporation step instead of long temperature-controlled aging conditions or hydrothermal processes. We believe these benefits coupled with the satisfactory photocatalytic activity and ease of separation from the reaction media (the ceramic powder that is to be separated in the case of 2 of the 3 synthesized samples are in the micrometer scale rather than nanoscale) may be a step forward in developing more sustainable photocatalysts for environmental applications.

**2. Experimental**

**2.1. Materials**

All chemicals and reagents were used as received without further purification. Chromatography grade microcrystalline cellulose was obtained from LubaChem (India). Pluronic P123 block copolymer (PEO-PPO-PEO) as structure directing agent was purchased from Sigma-Aldrich (United States). Titanium tetraisopropoxide C<sub>12</sub>H<sub>28</sub>O<sub>4</sub>Ti (TTIP) was obtained from DaeJung Company (South Korea). Absolute ethanol, methyl violet (MV), methyl orange (MO) and malachite green (MG) were purchased from Merck (Germany). Double distilled di-ionized water was used in all experiments.

**2.2. Instrumentation and characterization**

Powder X-ray diffraction patterns were recorded by Philips (Holland) PW1730 instrument using Cu-Kα irradiation (λ=1.5418 Å) and Rietveld refinement was performed with Materials

Table 1- Summary of selected reports in the field of sol-gel synthesis for titania nanomaterials

Entry	Method	Synthesis medium	Modulators/Additives	Results	Ref.
1	Sol-gel	Water/acetylacetone	KOH/HCl	Mesoporous particles	[9]
2	Sol-gel	EtOH <sup>*</sup>	KCl	Nanoporous particles	[10]
3	Sol-gel	EtOH	Hexadecylamine/water/KCl	Nanoporous microspheres	[11]
5	Sol-gel	Water	Isopropyl alcohol/HNO <sub>3</sub> or NaOH	Nanoparticles	[12]
6	Sol-gel	EtOH	HCl/diethanolamine Water+ EtOH for sol formation	Nanocrystalline powder	[13]
7	Sol-gel-hydrothermal	Water	Mineral acids/CTAB	Nanoparticles	[14]
8	EIS <sup>+</sup>	EtOH	HCl/water	Nanocrystals	[15]
9	EIS	EtOH	None/P123 Water/P123 None/P123+Cellulose	Nanoporous microspheres	This work

\*Ethanol

+ Evaporation Induced Self-assembly

Analysis Using Diffraction (MAUD) program [16-18]. Scanning electron microscopy (SEM) was performed on a TESCAN (Czech Republic) Vega. Field-emission scanning electron micrographs and EDS spectra and maps were obtained using a TESCAN (Czech Republic) Mira 3. Transmission electron microscopy was performed using holey carbon copper grids with a Philips (Holland) CM120 working at 100 kV as acceleration voltage. DLS spectra and zeta potentials were measured in water with a HORIBA (Japan) SZ-100 instrument. Diffuse reflectance spectroscopy (DRS) was performed with barium sulfate as blank standard on a Shimadzu (Japan) UV-2550 spectrophotometer and Kubeka-Monk method was used to determine the optical band-gap.

### 2.3. Synthesis of Titania samples

Titania was obtained via evaporation induced self-assembly (so called EIS) of pluronic P123 and titanium precursor (TTIP) in ethanol medium. In a typical run, 3 g of P123 was dissolved in 30 mL of absolute EtOH by vigorous magnetic stirring for 1 hour, afterwards, 4.5 mL of TTIP was added dropwise over the course of 15 minutes in order to avoid fast alcoholysis. The resulting clear sol was kept under reduced pressure at room temperature in order to remove the solvent. Calcination was performed at 500 °C (5 °C/min heating ramp) in a static air muffle furnace for 6 hr and then annealed to room temperature overnight. The obtained white powder was finely grounded using agate mortar and kept under reduced pressure until further characterization and photocatalytic activity evaluation, this sample coded as T0 (titania-zero conditions). Keeping all other parameters identical, the sample with the code TW was synthesized using 10:1 mixture of EtOH:water instead of the pure EtOH. Furthermore, in order to take use of the hard-soft templating approach, sample TC was synthesized by adding 200 mg of microcrystalline cellulose to the clear sol and vigorously stirring for another 1 hour before evaporation step.

### 2.4. Dye Removal Experiments

In a typical run, 5 mg of each sample was added to 20 mL of 10 ppm dye solution in a capped Pyrex<sup>®</sup> tube with a small Teflon<sup>®</sup> lined magnet inside. Magnetic stirring at 1000 rpm was applied for 30 minutes in darkness and then 60 minutes under illumination from a commercial 250 W high-pressure Hg lamp (NOOR-Osram, Iran). In

predetermined time intervals, 2 mL samples were taken from each reaction mixture and analyzed with visible spectrophotometry in transmission mode and then injected back to the mixture immediately. Baseline correction is needed especially for the sample TW (the mixture tends to become turbid due to small particle size).

### 3. Results and Discussion

Powder X-ray diffractometry was used to determine the phase content as well as crystallite size for the samples under study (Fig. 1). The T0 pre sample (before calcination) shows two distinct peaks at 18.95 and 23.12 diffraction angles which may be attributed to the discrete crystalline structure of pre-ceramic gel. Upon calcination, the structure is transformed to mainly anatase phase with tetragonal symmetry (PDF card no. 01-075-1537); the peaks observed at  $2\theta=25.07^\circ$ ,  $37.56^\circ$ ,  $48.83^\circ$ ,  $54.82^\circ$ ,  $55.99^\circ$  and  $63.19^\circ$  may be indexed as (101), (103), (200), (105), (211) and (213) respectively. The small peak which can be observed for T0 and TC at 27.40 is related to the (110) plane of rutile phase (PDF card no. 01-076-1939). In order to quantify the ratio of the aforementioned phases in each calcined sample, Rietveld refinement was used (table 2). According to most reports in the literature (for example see [19]), obtaining pure anatase phase via sol-gel approach requires pH modulation; slow alcoholysis and evaporation at room temperature can also give almost pure

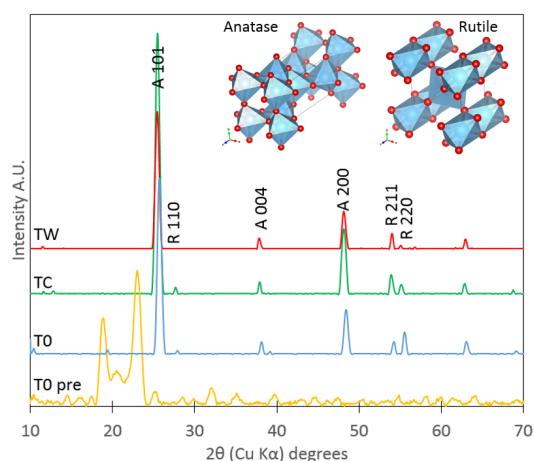


Fig. 1- Powder XRD patterns for the samples under study; T0 pre is the xerogel of T0 sample before calcination, T0 was synthesized with absolute EtOH, TW was synthesized with water as additional solvent and TC was obtained using microcrystalline cellulose as hard template. A and R represent the anatase and rutile crystalline phases respectively.

anatase phase. Addition of water (the case of TW sample) leads to even less rutile impurity (water is known promote the crystallization of amorphous titania into anatase [20]) but using cellulose as hard template would increase the formation of rutile; this may be attributed to its burnout and possible contribution of minor carbonous residues in the crystal nucleation and growth stage. Furthermore, as it can be seen in table 2, Scherrer's equation [21] was used to calculate the crystallite size of each sample based on the main anatase peak after computing the line broadening due to instrumentation by Warren's method [22]. Although the crystallite sizes of all three samples are in the same scale in accordance with TEM results (Fig. 4b), these would be the motifs which make markedly larger particles and pores depending on the synthesis conditions which is also proven by DLS result. Moreover, the zeta potentials of the samples under study were measured in water without pH modulation and they have all shown negative potentials in a scale sufficient for effective suspension formation for photocatalytic performance but not so much to hinder recovery of the particles after completion of

the degradation.

In order to gain more insight about the morphological evolution of the xerogel into anatase, field-emission scanning electron micrographs (Fig. 2) and EDS spectra (Fig. 3) were taken from both T0 pre and T0 samples. It is noteworthy that at first glance there is a significant difference between the morphology of xerogel and calcined ceramic (compare parts b and e in Fig. 2); formation of spherical ensembles from irregular shapes only with simple heat treatment seems highly unlikely. The aforementioned micrographs were obtained using secondary electron (SE) signal, but when signal was switched to backscattered electron detector (BSE), completely different morphological features were recorded (compare parts d and e in Fig. 2) which resembles that of the final ceramic. It can be postulated that the amount of P123 that can self-assemble with alcoholized titanium species in the synthesis conditions is limited, so that the remaining amount forms a thin organic cover on the surface of preceramic particles. This layer is thin enough so that the atomic number contrast of BSE micrographs is completely distinct from the

Table 2- Sample codes definition and summary of characterization results for the calcined samples (note that T0 pre is the xerogel obtained by solvent evaporation at room temperature)

Code	Synthesis conditions	Rietveld refinement		Scherrer crystallite size (nm)	DLS mean particle size (nm)	Mean Zeta potential (mV)	Total Removal efficiency (%) *		
		Anatase %	Rutile %				MV	MO	MG
T0	P123+EtOH	98.5	1.5	15	99.3±2.4	-33	77.9	25	55.8
TC	P123+EtOH+Cellulose	96.7	3.3	12	127.4±4.2	-31	92.5	7.8	45.6
TW	P123+EtOH:H <sub>2</sub> O (10:1)	99.2	0.8	15	283.8±34.7	-25	77.9	40.8	79.2

\* After 30 minutes in darkness and 60 minutes under illumination

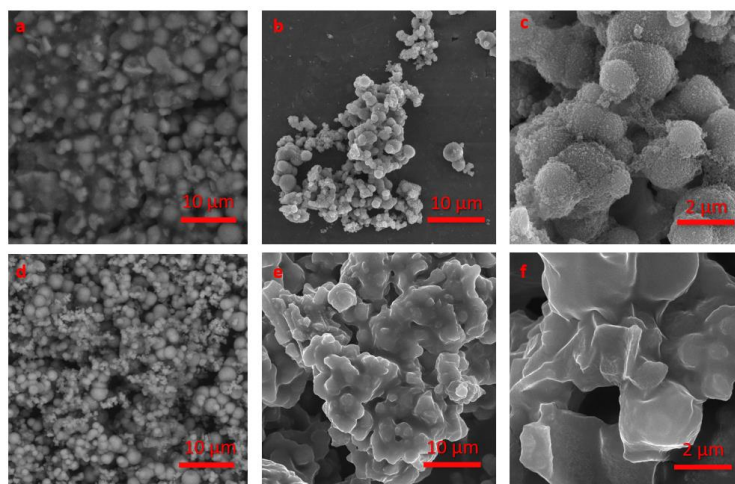


Fig. 2- Field-emission scanning electron micrographs for sample T0 (a-c) and T0 pre (d-e); the micrographs "a and d" are obtained with BSE signal and present atomic number contrast. More detailed explanation is provided in the text.

actual morphology seen in SE micrographs.

Elemental analysis on both T0 pre and T0 samples were performed by EDS method (parts a and b of Fig. 3). It's evident that the low energy peaks related to organics (P123) and oxygen are much stronger in the preceramic while the main peaks of titanium ( $K_{\alpha}$  and  $K_{\beta}$  characteristic radiations) become much more intense upon calcination. This is in agreement with the previously presented XRD results. Diffuse reflectance spectroscopy was also performed on T0 sample (part c of Fig. 3) and Kubelka-Munk (K-M) function [23] was plotted (part d of Fig. 3) for band-gap measurement. This function is based on total measured reflectance of a material ( $R_{\infty}$ ) and is defined as Eq. 1:

$$F(K - M) = \frac{(1 - R_{\infty})^2}{2R_{\infty}} \quad (1)$$

The reported band gaps for anatase and rutile are 3.2 and 3.0 eV, respectively [7] and the band positions are suitable for heterojunction formation when the two phases are in intimate contact (see the insert diagram of part d in Fig. 3). It's noteworthy that the measured optical band-gap for the sample T0 with only 1.5 wt.% rutile as heterojunction has

significantly decreased. Anatase has much higher adsorption capacity and an order of magnitude longer lifetime for the photogenerated electron and holes, so it can be postulated that most of charge carriers are concentrated on the more desirable anatase phase in the obtained photocatalyst and the photon absorption capacity is enhanced simultaneously compared to the pure anatase phase. This phenomenon leads to a considerable photocatalytic activity, which will be presented later on.

Thermodynamically, rutile is the stable phase of titania at room temperature and anatase is considered metastable [7]. Anatase can only be obtained in small particle sizes with high surface energy; if the particles grow to above 30 nm, anatase will transform to the more stable rutile [20]. The observed spherical ensembles in scanning electron micrographs (Fig. 2) are orders of magnitude larger than the aforementioned threshold and this would contradict the results of XRD phase and crystallite size analysis; thus, transmission electron microscopy was used to observe the crystallites directly. As it can be seen in Fig. 4a there are much smaller particles building up to form the micron-

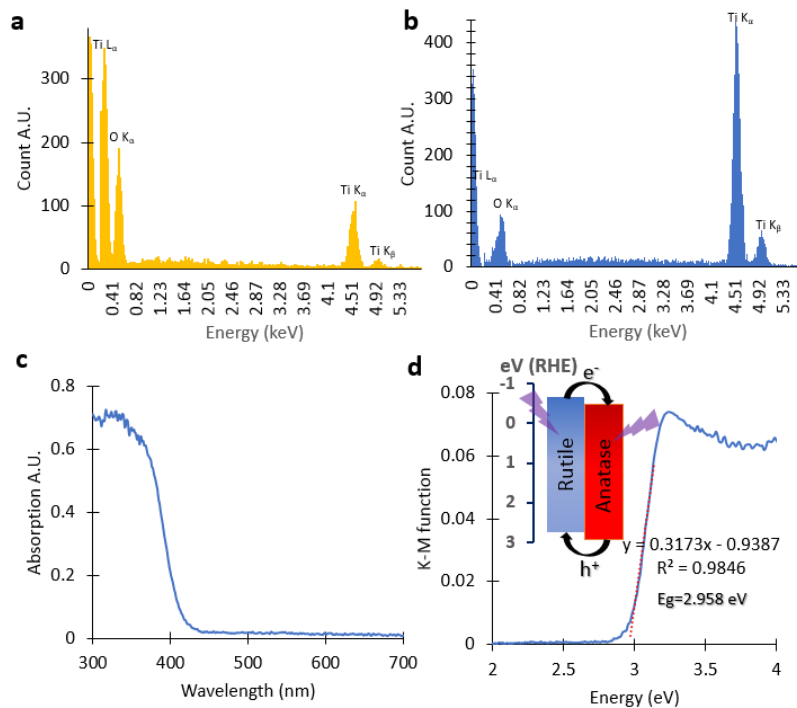


Fig. 3- EDS elemental analysis for samples T0 pre (a) and T0 (b); these spectra are obtained from the general locus of parts “a and d” in figure 2. Diffuse reflectance spectrum (c) as well as Kubelka-Munk curve (d) for the sample T0, insert of this part shows the band positions of anatase and rutile, detailed explanation can be found in text.

sized ensembles and nanopores are formed between these particles; this would have a profound effect in enhancing the contact area between reaction species and the solid photocatalyst because the observed pores are to a great extent larger than the diameter of organic dyes as model pollutants. Moreover, image analysis was used to measure particle size histogram (Fig. 4b); the mean particle diameter is measured to be 10 nm while the peak is observed at 7 nm, these values are in the same scale as the calculated crystallite size by Scherrer's formula and the discrepancy might be due to the deviation of crystallites from perfect spherical shape in this scale. Furthermore, DLS particle size distribution curves are presented in Fig. 4c. Comparing the field-emission scanning electron micrographs of sample T0 (e.g., Fig. 2c) to those of T0-pre (e.g., Fig. 2c), it's evident that a uniform layer of P123 is deposited on the ensembles of green ceramic right after solvent evaporation which is removed after calcination resulting in the formation of pores and breaking of the ensembles to some extent, nonetheless, the few nanometer sized crystallites lead to much larger particles in 100 nm scale. Addition of microcrystalline cellulose proved to have a minor effect on the crystallite size by acting as a secondary hard template, although the final particle size is essentially the same for this sample. Addition of water on the other hand had virtually no effect on the crystallite size, but it has a profound effect on the final powder size which can be attributed to the fast hydrolysis of titanium precursor compared to alcoholysis in absence of water; in such conditions a uniform layer of soft template cannot form and eventually separate the ensembles upon calcination.

Observation of pores in the nanostructure of T0 justifies the need for porosity analysis which

was performed by N<sub>2</sub>-physisorption at 77 K. The obtained adsorption-desorption isotherms are presented in part a of Fig. 5 for both TC and TW samples as the ones intended to be porous. Sample TC shows a type III standard class based on IUPAC, while TW sample shows type V behavior [24]. In the case of TC, no unrestricted monolayer formation is observed and the adsorbates are believed to have only weak interactions with the solid, clustering in the most favorable surface sites rather than covering the whole surface. It's also noteworthy that the amount of adsorbed probe is limited even at the saturation pressure, which means that the increase in the thickness of multilayers are indeed limited. In the case of TW sample with type V behavior, the first part of the isotherms is similar to that of type III (i.e. weak adsorbate-adsorbent interactions) but higher pressures lead to clustering and pore filling. The hysteresis loop of this sample resembles type H1 standard classification [24]; this steep and narrow loop shows delayed condensation which has been attributed to uniform mesospheres or ink-bottle pores. BET model was utilized to calculate the surface area of 14.2 and 29.5 m<sup>2</sup>g<sup>-1</sup> for TC and TW, respectively. Furthermore, total pore volumes of 0.06 and 0.35 cm<sup>3</sup>g<sup>-1</sup> were calculated for TC and TW, respectively. It is also noteworthy that the BJH peak radius (part b of Fig. 5) is exactly 2.4 nm for both samples. It can be postulated that the hard template (microcrystalline cellulose) did not disturb the spherical ensembles of anatase (compare the micrograph of part c in Fig. 5 with that of part a in Fig. 2, apart from larger particle sizes (critical in photocatalytic activity evaluation tests), the pores of this sample are still dominated by P123. On the other hand, addition of water leads to drastic microstructural changes (part d of Fig. 5) and formation of larger pores in the range of meso-

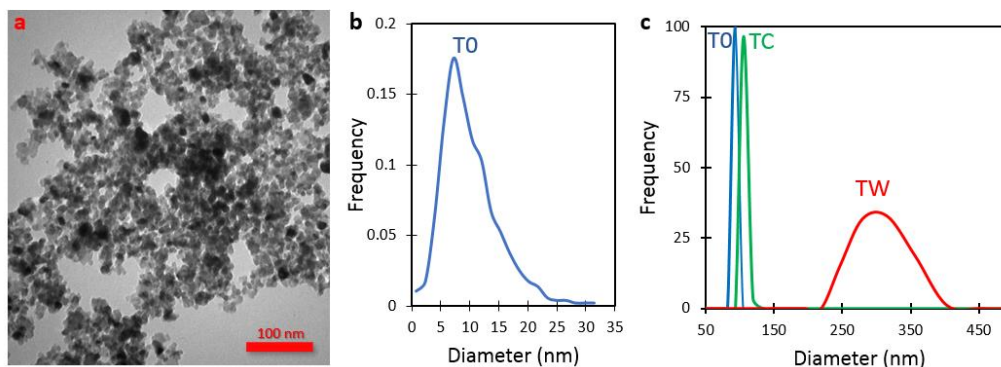


Fig. 4- Transmission electron micrographs (a and b) along with particle diameter histogram for the sample T0; note that the histogram was by image analysis on micrograph "a" and DLS particle size distribution curves for the three samples under study (c).

and macro-pores, but still the majority of pores are measured have exactly 2.4 nm radius; this suggests the presence of ink-bottle pores in accordance with the type of hysteresis observed for this sample as mentioned before.

The characterization results along with the literature suggest that the obtained titania samples may be fairly acceptable photocatalysts for removal of organic contaminants, especially dyes. Therefore, three different dyes were chosen,

namely, MG and MV as model cationic dyes and MO as a model anionic dye (table 3). Adsorption and photocatalytic activity depend upon acid-base properties of the powder to a great extent [25]. Molecular size and  $pK_a$  properties for the chosen dyes vary significantly, so it is expected that the hierarchical anatase nanostructures won't all be suitable for photodegradation of every single dye. This can mainly be attributed to the point of zero charge (PZC) which is reported to be 6 for anatase

Table 3- Chemical structure of the dyes under study for photocatalytic degradation

Dye name (type)	Chemical structure	$pK_a$	$\lambda_{max}$
Malachite green (Cationic)		10.3 [27]	617
Methyl violet (Cationic)		1.8 [28]	590
Methyl orange (Anionic)		4.46 [29]	465

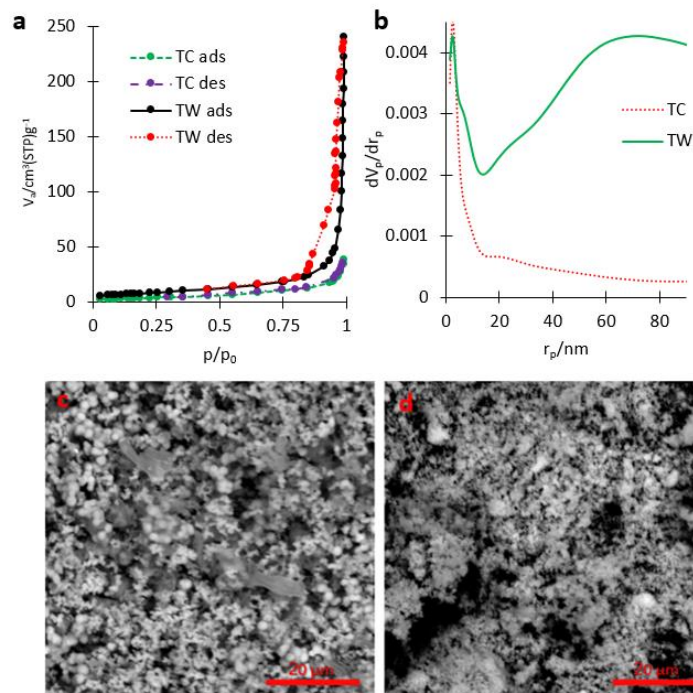


Fig. 5- $N_2$ -physorption isotherms (a) as well as BJH pore radius distribution curves (b) for the samples TC and TW. Scanning electron micrographs for the samples TC (c) and TW (d); note that both micrographs were obtained by BSE signal.

and 5.5 for rutile [26]. The PZC of obtained samples would probably be closer to that of anatase.

The results of dye removal experiments are summarized in Fig. 6; time dependent visible spectra were recorded and after baseline correction, the values of  $\lambda_{\max}$  were extracted in order to draw the diagrams of parts a-c in Fig. 6. It should be noted that the first 30 minutes of each experiment was performed in darkness, so the dye removal mechanism is solely the adsorption of dye molecules on the surface of titania particles. It is evident that none of the titania samples could remove methyl orange by adsorption (not even after 2 days of aging at darkness); this is due to the anionic nature of this dye. On the other hand, the best adsorption results are obtained with MV dye which may be attributed to the suitable  $pK_a$  in comparison to the PZC of titania, the best result was obtained for TC which was surprising when compared to the  $N_2$  porosimetry results. While TC has a lower surface area and total pore volume, the type of small mesopores (only 5.8 nm wide) seem to be suitable for providing multi-layer adsorption capacity, while this is not the same for the case of MG. With similar molecular size, the difference between MG and MV may be related to the difference in  $pK_a$ ; this property in the case of

MG is not suitable for adsorption on anatase, so that only the sample with the highest surface area (TW) shows a minor capacity in dye removal through adsorption for this particular dye. All samples have a similar set of microstructural properties including crystallite size and phase composition, but it should be noted that the TW sample has a much higher final aggregate size (evident by the DLS results) which is suitable for catalyst removal and re-use when considering it has offered the best results for removing two of the three dyes under study.

Total removal efficiency that is presented in part a of Fig. 7 is composed of both adsorption and photodegradation. A discussion similar to that presented for adsorption can be used to explain the difference between the samples under study for the photodegradation of various dyes. As can be seen, TW sample has worked best with both MG and MO while TC has worked better with MV, removing more than 90% of initial concentration in just 30 minutes of contact and 60 minutes of illumination. The different ratio of rutile-to-anatase phase doesn't seem to have a profound effect on the photocatalytic activity of the samples and they all seem to have benefited from heterojunction formation. Final degradation efficiencies of the

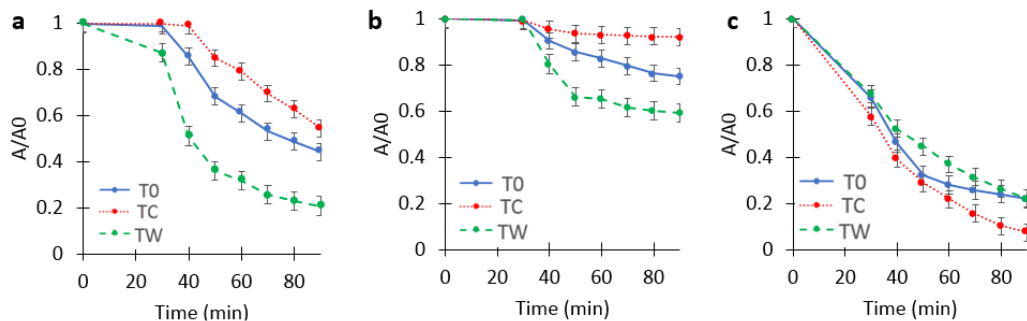


Fig. 6- Time-dependent degradation of three different organic dyes (a: MG, b: MO, c: MV) along with total degradation efficiency after 90 minutes (30 minutes dark, 60 minutes under illumination) for the samples under study.

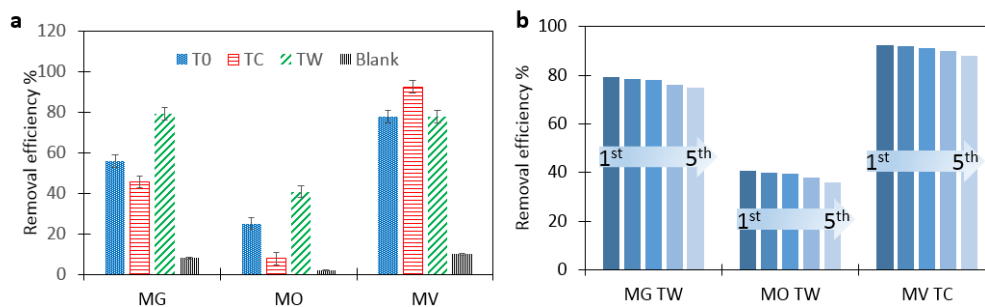


Fig. 7- a) overall removal efficiency (after 60 minutes of illumination) compared to blank tests performed without adding photocatalyst. b) recycling results for the optimized dye-photocatalyst pairs.

optimized dye/photocatalyst pairs are compared with the literature in table 4. As can be deduced from this table many dye concentrations and light sources were used in the past so it is best to compare the results of each material at the same conditions, but in a qualitative sense it is evident that the optimized dye/photocatalyst pairs are comparable to the best results from the literature.

Blank tests under similar conditions were also performed to evaluate the effect of illumination without using photocatalyst in dye degradation. Obtained results suggest that only a minute part of total degradation efficiency can be attributed to photolysis rather than photocatalytic degradation. This amount is highest for methyl violet and lowest for methyl orange.

Recycling experiments were performed by choosing the optimized dye/photocatalyst pairs. Each reaction run was terminated after 60 minutes of illumination and the photocatalyst was centrifuged, fresh dye solution with the same initial concentration was then added without washing the photocatalyst in order to imitate real application conditions and mitigate the photocatalyst loss due to recycling. The results of 5 consecutive reaction runs are presented in fig. 7b and they suggest that the photocatalysts under study can be considered as robust photodegradation materials for their intended dye.

#### 4. Conclusions

A simple evaporation induced self-assembly method was used to obtain porous anatase; morphology and surface chemistry can be rationally tailored by changing the reaction medium composition or using simple hard templates such as microcrystalline cellulose. These factors in turn determine the photocatalytic activity of the obtained sample toward different degradation dye types. Discrepancies amongst samples in terms of adsorption and photo-degradation of three representative organic pollutants were attributed to the surface chemistry of each sample compared to the  $pK_a$  of the dyes making possible the engineering of the porous titania samples for each intended pollutant. Based on Rietveld refinement, the synthesized titania samples have between 0.8 to 3.3 wt.% rutile phase impurity which can effectively form a heterojunction with anatase and reduce the optical band gap from the theoretical 3.2 eV to less than 3.0 eV even in such low contents making this environmentally friendly material more efficient in pure form. The presented approach can be utilized to other types of oxide as well as mixed-oxide ceramics for a variety of applications and further efforts are currently underway to develop its scope.

#### 5. Statements and Declarations

There are no Conflict of Interests in this article.

Table 4- summary of representative results from the literature concerning the photocatalytic degradation of the organic dyes under study with TiO<sub>2</sub> based materials

Entry	Composition (ppm)	Light source	Dye (concentration)	Degradation efficiency (minutes)	Ref.
1	TiO <sub>2</sub> (coating)	Visible with 400 nm cutoff	MG <sup>2</sup> (5 ppm)	60% (100)	[30]
2	Fe:TiO <sub>2</sub> (coating)	Visible with 400 nm cutoff	MG <sup>2</sup> (5 ppm)	75% (100)	[30]
3	Au:TiO <sub>2</sub> (2000)	UVA	MG (10 <sup>-5</sup> M)	95% (120)	[31]
4	Ni:TiO <sub>2</sub> (1200)	Solar	MG (250 ppm)	~100 (180)	[32]
5	Co:TiO <sub>2</sub>	Solar	MG (50 ppm)	82.3 (180)	[33]
6	TiO <sub>2</sub> (500)	UVA	MG (50 ppm)	93 (360)	[34]
7	TiO <sub>2</sub> (100)	Hg 125W	MG (5×10 <sup>-5</sup> M)	98 (120)	[35]
8	TiO <sub>2</sub> (250)	Hg 250W with UV filter	MG (10 ppm)	79 (60)	TW
9	TiO <sub>2</sub>	Hg 125 W	MO (3.2×10 <sup>-3</sup> M)	90% (120) with H <sub>2</sub> O <sub>2</sub>	[36]
10	TiO <sub>2</sub> (2000)	UV 40W	MO (10 <sup>-3</sup> M)	80 (200)	[37]
11	TiO <sub>2</sub> /carbon (2000)	UV 40W	MO (10 <sup>-3</sup> M)	100 (130)	[37]
12	TiO <sub>2</sub> (250)	Hg 250W with UV filter	MO (10 ppm)	40.8 (60)	TW
13	TiO <sub>2</sub>	UV 16W	MV (5×10 <sup>-5</sup> M)	70% (90)	[38]
14	Ag:TiO <sub>2</sub>	UV 16W	MV (5×10 <sup>-5</sup> M)	>99% (90)	[38]
15	TiO <sub>2</sub> (2000)	UVB 15W	MV (15ppm)	35% (20)	[39]
16	Pd:TiO <sub>2</sub> (2000)	UVB 15W	MV (15ppm)	98% (20)	[39]
17	Pt:TiO <sub>2</sub> (2000)	UVB 15W	MV (15ppm)	78% (20)	[39]
18	TiO <sub>2</sub> (250)	Hg 250 W with UV filter	MV (10 ppm)	92.5 (60)	TC

## References

- Han F, Kambala VSR, Srinivasan M, Rajarathnam D, Naidu R. Tailored titanium dioxide photocatalysts for the degradation of organic dyes in wastewater treatment: A review. *Applied Catalysis A: General*. 2009;359(1-2):25-40.
- Allen SJ, Koumanova B. Decolourisation of water/wastewater using adsorption. *Journal of the university of chemical technology and metallurgy*. 2005 Jul;40(3):175-92.
- Aplin R, Waite TD. Comparison of three advanced oxidation processes for degradation of textile dyes. *Water Science and Technology*. 2000;42(5-6):345-54.
- Rauf MA, Ashraf SS. Fundamental principles and application of heterogeneous photocatalytic degradation of dyes in solution. *Chemical Engineering Journal*. 2009;151(1-3):10-8.
- Fujishima A, Rao TN, Tryk DA. Titanium dioxide photocatalysis. *Journal of Photochemistry and Photobiology C: Photochemistry Reviews*. 2000;1(1):1-21.
- Daghrir R, Drogui P, Robert D. Modified TiO<sub>2</sub> For Environmental Photocatalytic Applications: A Review. *Industrial & Engineering Chemistry Research*. 2013;52(10):3581-99.
- Zhang J, Zhou P, Liu J, Yu J. New understanding of the difference of photocatalytic activity among anatase, rutile and brookite TiO<sub>2</sub>. *Physical Chemistry Chemical Physics*. 2014;16(38):20382-6.
- Akpan UG, Hameed BH. The advancements in sol-gel method of doped-TiO<sub>2</sub> photocatalysts. *Applied Catalysis A: General*. 2010;375(1):1-11.
- Antonelli DM, Ying JY. Synthesis of Hexagonally Packed Mesoporous TiO<sub>2</sub> by a Modified Sol-Gel Method. *Angewandte Chemie International Edition in English*. 1995;34(18):2014-7.
- Ren W, Ai Z, Jia F, Zhang L, Fan X, Zou Z. Low temperature preparation and visible light photocatalytic activity of mesoporous carbon-doped crystalline TiO<sub>2</sub>. *Applied Catalysis B: Environmental*. 2007;69(3-4):138-44.
- Chen D, Cao L, Huang F, Imperia P, Cheng Y-B, Caruso RA. Synthesis of Monodisperse Mesoporous Titania Beads with Controllable Diameter, High Surface Areas, and Variable Pore Diameters (14–23 nm). *Journal of the American Chemical Society*. 2010;132(12):4438-44.
- Siti Aida I, Srimala S. Effect of pH on TiO<sub>2</sub> nanoparticles via sol gel method.
- Tsega M, Dejene FB. Influence of acidic pH on the formulation of TiO<sub>2</sub> nanocrystalline powders with enhanced photoluminescence property. *Heliyon*. 2017;3(2):e00246-e.
- Xu H, SoNo Z, XUDoNo WA, HAo WA. Synthesis of Well-Dispersed TiO<sub>2</sub> Nanoparticles by a Sol-Hydrothermal Method. *Asian Journal of Chemistry*. 2011 May 1;23(5):2339-42.
- Sharma R, Sarkar A, Jha R, Kumar Sharma A, Sharma D. Sol-gel-mediated synthesis of TiO<sub>2</sub> nanocrystals: Structural, optical, and electrochemical properties. *International Journal of Applied Ceramic Technology*. 2020;17(3):1400-9.
- Lutterotti L. Total pattern fitting for the combined size-strain-stress-texture determination in thin film diffraction. *Nuclear Instruments and Methods in Physics Research Section B: Beam Interactions with Materials and Atoms*. 2010;268(3-4):334-40.
- Lutterotti L. Maud: a Rietveld analysis program designed for the internet and experiment integration. *Acta Crystallographica Section A Foundations of Crystallography*. 2000;56(s1):s54-s.
- Lutterotti L, Matthies S, Wenk HR, Schultz AS, Richardson JW. Combined texture and structure analysis of deformed limestone from time-of-flight neutron diffraction spectra. *Journal of Applied Physics*. 1997;81(2):594-600.
- Sugimoto T, Zhou X. Synthesis of Uniform Anatase TiO<sub>2</sub> Nanoparticles by the Gel-Sol Method. *Journal of Colloid and Interface Science*. 2002;252(2):347-53.
- Reyes-Coronado D, Rodríguez-Gattorno G, Espinosa-Pesqueira ME, Cab C, de Coss R, Oskam G. Phase-pure TiO<sub>2</sub> nanoparticles: anatase, brookite and rutile. *Nanotechnology*. 2008;19(14):145605.
- Scherrer, P., *Nachrichten von der Gesellschaft der Wissenschaften zu Göttingen. Mathematisch-Physikalische Klasse*, 1918. 2: p. 98-100.
- Khayati GR, Janghorban K. The nanostructure evolution of Ag powder synthesized by high energy ball milling. *Advanced Powder Technology*. 2012;23(3):393-7.
- Kubelka P. Ein Beitrag zur Optik der Farbanstriche (Contribution to the optic of paint). *Zeitschrift für technische Physik*. 1931;12:593-601.
- Thommes M, Kaneko K, Neimark AV, Olivier JP, Rodriguez-Reinoso F, Rouquerol J, et al. Physisorption of gases, with special reference to the evaluation of surface area and pore size distribution (IUPAC Technical Report). *Pure and Applied Chemistry*. 2015;87(9-10):1051-69.
- Paola AD, Ikeda S, Marci G, Ohtani B, Palmisano L. Transition metal doped: physical properties and photocatalytic behaviour. *International Journal of Photoenergy*. 2001;3(4):171-6.
- Kosmulski M. The significance of the difference in the point of zero charge between rutile and anatase. *Advances in Colloid and Interface Science*. 2002;99(3):255-64.
- Swan NB, Zaini MAA. Adsorption of Malachite Green and Congo Red Dyes from Water: Recent Progress and Future Outlook. *Ecological Chemistry and Engineering S*. 2019;26(1):119-32.
- Adams EQ, Rosenstein L. The Color and Ionization of Crystal-Violet. *Journal of the American Chemical Society*. 1914;36(7):1452-73.
- de Oliveira HP. Determination of pKa of dyes by electrical impedance spectroscopy. *Microchemical Journal*. 2008;88(1):32-7.
- Asiltürk M, Sayılkan F, Arpaç E. Effect of Fe<sup>3+</sup> ion doping to TiO<sub>2</sub> on the photocatalytic degradation of Malachite Green dye under UV and vis-irradiation. *Journal of Photochemistry and Photobiology A: Chemistry*. 2009;203(1):64-71.
- Abd-Rabboh HSM, Benaissa M, Ahmed MA, Fawy KF, Hamdy MS. Facile synthesis of spherical Au/TiO<sub>2</sub> nanoparticles by sol-gel method using Tween 80 for photocatalytic decolorization of Malachite Green dye. *Materials Research Express*. 2018;6(2):025028.
- Pirsaheb M, Shahmoradi B, Khosravi T, Karimi K, Zandsalimi Y. Solar degradation of malachite green using nickel-doped TiO<sub>2</sub> nanocatalysts. *Desalination and Water Treatment*. 2016;57(21):9881-8.
- Kamble RJ, Gaikwad PV, Garadkar KM, Sabale SR, Puri VR, Mahajan SS. Photocatalytic degradation of malachite green using hydrothermally synthesized cobalt-doped TiO<sub>2</sub> nanoparticles. *Journal of the Iranian Chemical Society*. 2022;19(1):303-12.
- Chen C, Lu C, Chung Y, Jan J. UV light induced photodegradation of malachite green on TiO<sub>2</sub> nanoparticles. *Journal of Hazardous Materials*. 2007;141(3):520-8.
- Prado AGS, Costa LL. Photocatalytic decoloration of malachite green dye by application of TiO<sub>2</sub> nanotubes. *Journal of Hazardous Materials*. 2009;169(1-3):297-301.
- Yang H, Zhang K, Shi R, Li X, Dong X, Yu Y. Sol-gel synthesis of TiO<sub>2</sub> nanoparticles and photocatalytic degradation of methyl orange in aqueous TiO<sub>2</sub> suspensions. *Journal of Alloys and Compounds*. 2006;413(1-2):302-6.
- Li Y, Li X, Li J, Yin J. Photocatalytic degradation of methyl orange by TiO<sub>2</sub>-coated activated carbon and kinetic study. *Water*

Research. 2006;40(6):1119-26.

38. Gupta AK, Pal A, Sahoo C. Photocatalytic degradation of a mixture of Crystal Violet (Basic Violet 3) and Methyl Red dye in aqueous suspensions using Ag<sup>+</sup> doped TiO<sub>2</sub>. *Dyes and*

*Pigments*. 2006;69(3):224-32.

39. Saeed K, Khan I, Gul T, Sadiq M. Efficient photodegradation of methyl violet dye using TiO<sub>2</sub>/Pt and TiO<sub>2</sub>/Pd photocatalysts. *Applied Water Science*. 2017;7(7):3841-8.